J Mater Sci: Mater Med (2011) 22:279–288
DOI 10.1007/s10856-010-4194-2

Fabrication of chitosan/poly(ε-caprolactone) composite hydrogels for tissue engineering applications

Xia Zhong · Chengdong Ji · Andrew K. L. Chan · Sergei G. Kazarian · Andrew Ruys · Fariba Dehghani

Received: 20 July 2010 / Accepted: 19 November 2010 / Published online: 19 December 2010

Abstract The aim of this study was to fabricate three-dimensional (3D) porous chitosan/poly(ε-caprolactone) (PCL) hydrogels with improved mechanical properties for tissue engineering applications. A modified emulsion lyophilisation technique was developed to produce 3D chitosan/PCL hydrogels. The addition of 25 and 50 wt% of PCL into chitosan substantially enhanced the compressive strength of composite hydrogel 160 and 290%, respectively, compared to pure chitosan hydrogel. The result of ATR–FTIR imaging corroborated that PCL and chitosan were well mixed and physically co-existed in the composite structures. The composite hydrogels were constructed of homogenous structure with average pore size of 59.7 ± 14 μm and finer pores with average size of 4.4 ± 2 μm on the wall of these larger pores. The SEM and confocal laser scanning microscopy images confirmed that fibroblast cells were attached and proliferated on the 3D structure of these composite hydrogels. The composite hydrogels acquired in this study possessed homogeneous porous structure with improved mechanical strength and integrity. They may have a high potential for the production of 3D hydrogels for tissue engineering applications.

Xia Zhong and Chengdong Ji contributed equally and share the first authorship.

X. Zhong · C. Ji · F. Dehghani (✉)
School of Chemical and Biomolecular Engineering, University of Sydney, Sydney, Australia
e-mail: fariba.dehghani@sydney.edu.au

A. K. L. Chan · S. G. Kazarian
Department of Chemical Engineering, Imperial College London, London, UK

A. Ruys
School of Aerospace, Mechanical and Mechatronic Engineering, University of Sydney, Sydney, Australia

1 Introduction

The fabrication of a three-dimensional (3D) hydrogel plays a significant role in tissue engineering. Hydrogel provides a template for cell adhesion and proliferation, and subsequently extracellular matrix (ECM) formation [1, 2]. However, few biomaterials possess all the desirable properties such as mechanical strength and cell affinity for tissue engineering applications. Blending hydrophilic and hydrophobic polymers has been demonstrated to be an efficient strategy to develop new biomaterials exhibiting combinations of properties that could not be acquired by individual materials [3, 4]. Usually synthetic hydrophobic polymers have superior mechanical strength but lack of cell-recognition signals and their hydrophobic surface properties hamper the cell adhesion, which can be complemented by mixing with natural polymers having excellent biocompatibility [3]. Cell adhesion and proliferation of poly(lactide-*co*-glycolide) (PLGA) were promoted by blending it with collagen, and the resulting composite hydrogel exhibited higher mechanical strength than pure collagen sample [5].

Chitosan, a partially deacetylated derivative of chitin, has been used in tissue engineering applications because of its hydrophilicity, biocompatibility, biodegradability, non-toxicity, affinity to proteins and anti-microbial properties [6]. However, chitosan exhibits relatively low mechanical strength; in wet state the extensibility (maximum strain) of non-porous chitosan membrane is only 30%, which impedes its broad applications [6, 7]. Poly(ε-caprolactone) (PCL) is biodegradable and biocompatible polyester with

excellent mechanical strength. The elongation of PCL membranes is up to 1000% before break [3, 8]. Nevertheless, the usage of PCL in tissue engineering is restricted due to the poor bioregulatory activity and slow degradation rate [9, 10]. The PCL/chitosan composites may address the individual problem associated with each of these polymers.

It is a major problem to find a common solvent to dissolve both PCL and chitosan for the preparation of homogenous composite, because chitosan is only soluble in acidic solution and PCL dissolves in organic solvents such as dichloromethane and chloroform that are not miscible with water. It is also not feasible to melt chitosan and blend it with PCL [3, 7, 11]. Recently, hexafluoro-2-propanol (HFIP) and also concentrated acetic acid (over 77%) were used to dissolve both PCL and chitosan; a thin membrane that had low porosity was produced by solvent evaporation [4, 12]. This 2D structure is not desirable for most tissue engineering applications due to lack of pore interconnectivity. Porous hydrogels were fabricated with different techniques such as salt leaching and freeze drying based on these single phase solutions [3, 4, 11–15]. Sarasam et al. [14] mixed chitosan and PCL in 77% acetic acid, and attempted to fabricate 3D composite hydrogels by freeze drying technique. However, PCL/chitosan composite acquired poor structural integrity, which was resulted from the phase behavior of concentrated acetic acid [3].

Emulsion freeze drying has been used to prepare the 3D porous composites from PCL and hydrophilic polyvinyl alcohol (PVA) [16]. High speed mechanical stirring was used to generate the emulsion from PVA aqueous solution and PCL dichloromethane solution. Porous composite hydrogels were produced with pore size between 30 and 300 μm and compressive modulus above 1.5 MPa [16].

In this study emulsion freeze drying technique was selected to fabricate chitosan/PCL composite hydrogels. Sonication technique was applied to prepare homogeneous emulsion. The effect of PCL concentration on the characteristics of composite hydrogels such as mechanical strength, swelling property, and uniformity was determined. In vitro tests were conducted to investigate the biocompatibility of composite hydrogels and assess cell infiltration in 3D structure.

2 Materials and methods

2.1 Materials

Chitosan (medium molecular weight), poly(ε-caprolactone) (PCL), fluorescein diacetate (FDA), propidium iodide (PI), Dulbecco's modified eagle medium (DMEM), fetal bovine serum (FBS), pen-strep and sorbitan monooleate (Span-80) were purchased from Sigma. Dichloromethane (DCM) (99.4% purity), ethanol (99.7% purity) and sodium hydroxide (NaOH) were purchased from Merck. A 0.2 M acetic acid solution was prepared using glacial acetic acid (Ajax Fine Chem) in MilliQ water.

2.2 Fabrication of chitosan/PCL composite hydrogels

Solution of chitosan (1.5 w/v%) in 0.2 M acetic acid and PCL (5 w/v%) in DCM were prepared. Different volume ratios of chitosan/PCL solutions were mixed by using span-80 (5 v/v% of the total solution volume) as an emulsifier, followed by sonication (Hielschar UP400S) at 20 mV for 2 min to achieve homogenous emulsion. The ultrasound power and time were optimised to generate stable, homogenous emulsion, and prevent undesirable effect on chemical integrity of chemicals. The emulsion mixture was then immediately poured into custom-made glass mould (1 cm diameter), and frozen at −20°C overnight, followed by lyophilisation for at least 2 days. The lyophilized hydrogels were immersed into 0.2 M NaOH for 2 h to neutralize the acid residues and then washed three times with MilliQ water. The hydrogels were lyophilized again overnight prior to further characterization. The control in this study was prepared by lyophilisation of chitosan (1.5 w/v%) in 0.2 M acetic acid aqueous solution.

2.3 Characterisations

2.3.1 Scanning electron microscopy (SEM)

The microstructure of the composite hydrogels was examined by SEM (Philips XL30). Prior to SEM analysis (15 kV), dried sample was sputter-coated with 10 nm gold. Equivalent circle diameter (ECD) of the pores was calculated by using Image J software. In brief, the pores were manually picked by built-in drawing functions, and the area (A) of each pore was subsequently measured by using 'Measure' function. The pore diameter was then calculated according to following formula: $d = \sqrt{4A/\pi}$

To validate this measurement statistically, at least five images (300 pores) with same magnification representing different areas of the hydrogel were analysed at each condition.

2.3.2 Equilibrium swelling ratio

The equilibrium swelling ratio (S_w) of the composite hydrogels was determined at physiological environment. In brief, the dried hydrogel was cut into similar size ($\sim 1 \times 1 \times 1$ cm^3) and weighted (W_0). At each condition three samples were immersed into pre-warmed PBS at 37°C overnight (at least 12 h). The swollen samples were

weighted (W_t) after excessive buffer was removed. The equilibrium swelling ratio was calculated using the equation $S_w = (W_t - W_0)/W_0$.

2.3.3 Fourier transform infrared (FTIR) spectroscopy

The existence of each component in the composites and potential molecular interactions were determined with Attenuated Total Reflectance-Fourier Transform Infrared spectroscopy (ATR–FTIR) (Varian 660-IR) at 4 cm^{-1} resolution over the range 600–4000 cm^{-1} wavenumber. FTIR images were collected with the system that comprises of continuous scan FTIR spectrometer, a large sample compartment, and a 128 × 128 focal plane array (FPA) detector. The diamond ATR-IR accessory was positioned in the sample compartment and carefully aligned prior to the measurements [17–21]. Only 6,400 (80 × 80) of the FPA detector pixels were used in this measurement. The sample area measured by this macro-ATR imaging approach was ca. 0.7 × 1.0 mm^2. A spectral resolution of 8 cm^{-1} was used in this study. Thirty-two scans were collected in each imaging measurement.

2.3.4 Mechanical test

Uniaxial compression tests of hydrated specimens were performed by using a Bose ELF 3400 mechanical tester. Prior to mechanical test, the composite hydrogels were immersed into PBS for 2 h. The thickness (~3 mm) and diameter (~8 mm) of each sample were measured using a digital calliper (J.B.S). A cell load with 50 N, cross head speed of 30 μm/s and 50% strain level were applied. The compressive modulus was obtained as the tangent slope of the stress–strain curve. The tensile property of the composite hydrogel was examined by using dynamic mechanical analyser (DMA, TA Instrument, 2980). The samples were cut into dumbbell shape (~7 × 5 × 1, length × width × thickness in mm) ($n = 3$). A constant strain rate (0.5%) was applied on the sample. The stress (MPa) was recorded by built-in software and the tensile modulus was calculated as the tangent slope of the linear region of the stress–strain curve.

2.3.5 In vitro cell culturing test

In vitro cell culturing test was carried out to assess the biocompatibility of the composite hydrogel for tissue engineering applications. The composites were transferred into a 24-well plate and sterilized, and then immersed in culture media (DMEM, 10% FBS, 1% pen-strep) at 37°C overnight. The cells (human skin fibroblast cells GM3348) were then seeded onto the hydrogels at 3 × 10^5 cells/well by using pipette tips and cultured in an incubator at 37°C in the presence of 5% CO_2 and 95% humidity for 7 days. The media was refreshed every 3 days. Hydrogels with cell cultured for 3 and 7 days were stained with FDA and PI, respectively, and assessed by confocal laser scanning microscopy (CLSM, Nikon Limo). Live cells were stained fluorescent green due to intracellular esterase activity that de-acetylated FDA to a green fluorescent product. Dead cells were stained fluorescent red as their compromised membranes were permeable to nucleic acid stain PI.

3 Results and discussion

3.1 Fabrication of chitosan/PCL hydrogels

Homogeneous stable emulsions of chitosan and PCL solutions were prepared, rapidly, using sonication-assisted emulsification. This method was more efficient than mechanical agitation in creating the micron size droplet of a lean phase in the continuous polymer rich phase at a shorter processing time [22]. It can be seen that homogeneous milky emulsion formed after only two minutes sonication (Fig. 1a, b) using 5 v/v% Span-80 as an emulsifier. Without the addition of emulsifier, as shown in Fig. 1c, phase separation occurred in the solution after

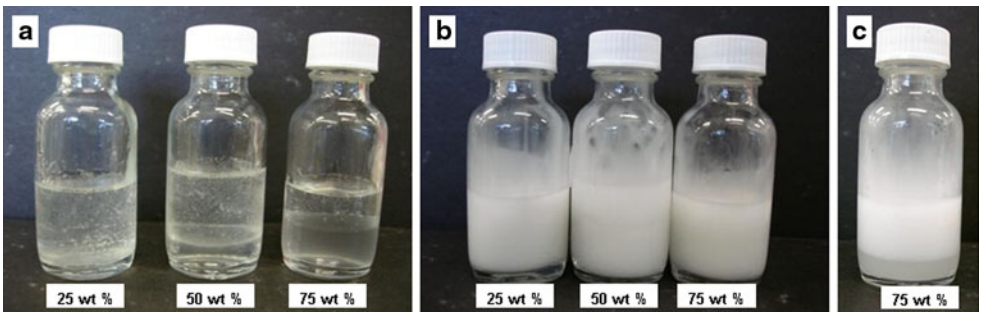

Fig. 1 Chitosan/PCL emulsion with different PCL composition (25, 50, 75 wt%): **a** solutions before sonication (The upper layer is chitosan solution and the lower one is PCL solution); **b** emulsion solution after sonication with surfactant; **c** emulsion solution after sonication without surfactant

15 min, which was undesirable for the fabrication of composite hydrogels.

PCL/chitosan scaffolds with homogenous and rigid 3D structure were fabricated containing less than 50 wt% PCL by lyophilisation of emulsion solution prepared by sonication. As shown in Fig. 2, when using 75 wt% PCL an irregular shape and fragile scaffolds was formed. When the PCL composition was not more than 50 wt%, the emulsion system of PCL DCM solution and chitosan acetic acid solution was stable during the freezing and lyophilisation process. Namely, the PCL solution droplets dispersed uniformly in the chitosan acetic acid solution phase. After the emulsion was frozen at −20°C, the chitosan acetic acid solution turned into ice phase, however, due to the low melting point of DCM (−96°C), the PCL solution remained as liquid phase. During the lyophilisation, the ice sublimated under vacuum conditions resulting in the formation of macro pores, meanwhile, the DCM was evaporated which generated the micro pores as shown in Fig. 3c–f. When the PCL composition was increased up to 75 wt%, the volume ratio of continuous phase, which was chitosan acetic acid solution and dispersed phase, which was PCL solution in this case was close to or even above the emulsion system phase inversion point. By definition, the phase inversion point is the holdup of the dispersed phase for a system at which the transition occurs, that is, when the dispersed phase becomes the continuous phase after an infinitesimal change is made to the system's properties, phase ratio or energy input [23, 24]. Therefore, the PCL solution droplets began coalescing and entrapped chitosan acetic acid solution into droplets to further form PCL/DCM continuous phase. After drying, the powdery structure of composite containing 75 wt% PCL was formed. As shown in Fig. 3g, h, the composite presented regular micro pores which was generated from the lyophilisation of the inversed chitosan acetic acid solution droplets, however, macro pores was not present and PCL existed as bulk pieces which resulted in the loss of mechanical strength and structural integrity. Therefore, the composites with 25 and 50 wt% PCL that possessed firm structure were selected for further characterizations.

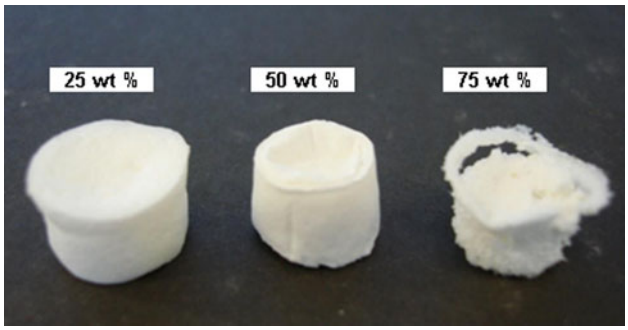

Fig. 2 The structure of chitosan/PCL composites at various compositions

3.2 Structural morphology of composite hydrogels

Composite hydrogels with homogeneous porous structures were formed using the method developed in this study (Fig. 3). The average pore size was decreased from 137 μm for neat chitosan to 60 μm for both 25 and 50 wt% PCL as depicted in Table 1. The pore size of pure chitosan hydrogel fabricated in this study was consistent with the data reported in the literature [25]. However, the addition of DCM phase in the emulsion system may create different thermal gradients compared to pure chitosan aqueous solution and resulted in generation of smaller pore size.

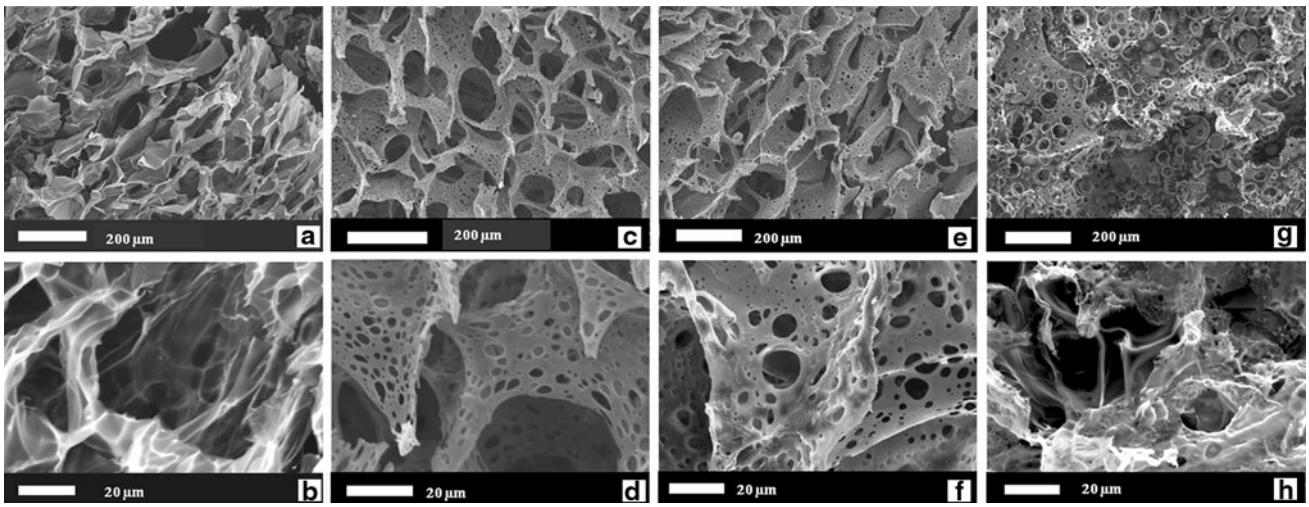

Fig. 3 SEM images of **a**, **b** pure chitosan, composite hydrogels **c**, **d** 25 wt% PCL **e**, **f** 50 wt% PCL and **g**, **h** 75 wt% PCL

Table 1 Pore sizes and swelling ratio of the composite hydrogels

Chitosan/PCL (wt%)	Macropore diameter (μm)	Micropore diameter (μm)
100/0	136.9 ± 39.4	N/A
75/25	57.9 ± 12.5	4.4 ± 1.5
50/50	65.5 ± 13.2	7.1 ± 3.5

The effect of freezing temperature prior to lyophilisation on the pore size was examined. Freezing the emulsion solution with liquid nitrogen at −196°C resulted in fabricating smaller size pores in composite hydrogel with average diameters less than 20 μm, which may not be desirable for tissue engineering; when −20°C was used for sample freezing, larger pores could be achieved (Fig. 4). The results of previous study also demonstrated that decreasing the freezing temperature from −20 to −80°C reduce the pore size of hydrogels from 121 to 15 μm [7, 26, 27]. It is believed that during the freezing process, ice crystals nucleate from solution and grow along the lines of thermal gradients, which leads to the various pore sizes from different freezing temperatures. Therefore, pore size can be controlled by the ice crystal size via varying the freezing rate [6]. In this study, to achieve the desired pore size for further cell culture, −20°C was selected as the freezing temperature.

The major feature in these composite hydrogels was the formation of fine pores (less than 10 μm) on the macro pore walls (Fig. 3c–f). These pores may be generated from the evaporation of organic solvents during freeze drying process (lyophilisation). The droplet of organic phase containing PCL was dispersed into the continuous phase of frozen aqueous chitosan solution, because the freezing point of DCM (−96°C) was below the freezing temperature (−20°C) used prior to freeze drying. Considering the possible effect of sample thickness on DCM evaporation, the dimension of all the samples prepared in this study was kept consistent (1 cm diameter and 0.8 cm height). SEM examination demonstrated that there was no observable difference of pore morphology with the top surface, cross section and bottom section.

As shown in Table 1, the average diameter of pores on the walls were 4.4 and 7.1 μm for 25 wt% PCL and 50 wt% PCL, respectively. This effect may be resulted from the difference in viscosity of the solutions; increasing the PCL concentration, enhanced the viscosity of solution, subsequently larger droplets of the lean phase were created during the emulsion process. Larger pores may also be formed as a result of increasing the density of droplets and their coalescences at higher concentration. The organic solvent droplet formed from sonication process was covered with the surfactant monolayer and the morphology of the droplet was affected by the hydrophobicity of the system. Increasing the hydrophobicity dilates the dimensions of the hydrophobic droplets to optimise the particle free energy and surface tension [28]. Increasing the PCL concentration from 25 to 50 wt% increased the hydrophobicity of the emulsion and enlarged the size of hydrophobic droplets twofold. The presence of these pores may increase oxygen, nutrient and waste transfer for cell growth in these composite hydrogels compared with pure chitosan hydrogels.

3.3 ATR–FTIR spectroscopic analysis

Fourier Transform Infrared (FTIR) spectroscopy (Varian 660-IR) was used to determine the presence of each component in the composites and their potential molecular interactions. The FTIR spectra of the typical absorption peaks of the functional groups present in chitosan and PCL are shown in Fig. 5. Pure chitosan has a peak absorbance at 1,560 cm^{-1}, which corresponds to the N–H band for either primary amines or amide II, and another peak was detected at 1,659 cm^{-1}, corresponding to the C=O stretch for amide I, which indicated that chitosan was not completely deacetylated [29]. The prominent characteristic peak of PCL locates at about 1,724 cm^{-1}, attributed to the carbonyl group stretching absorption [30]. As expected, all the characteristic peaks of chitosan and PCL were observed in FTIR spectra of chitosan/PCL composite, which corroborates the existence of both components in the composite structures (Fig. 5). Characteristic peaks of chitosan were more distinguishable in the spectrum containing 25 wt%

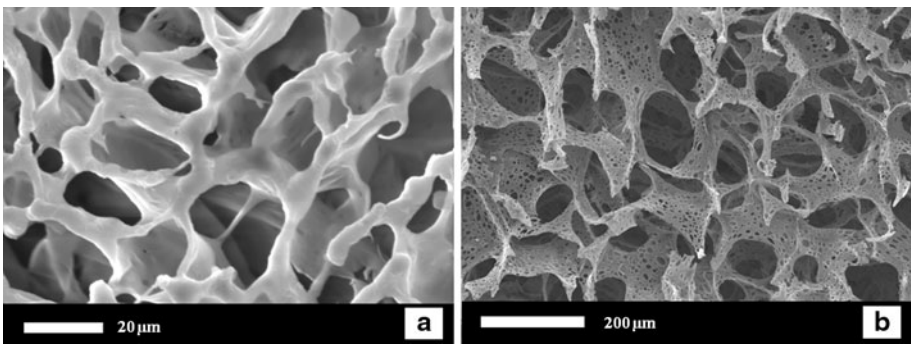

Fig. 4 SEM images of composite hydrogel containing 25 wt% PCL frozen at **a** liquid nitrogen (−196°C) and **b** −20°C

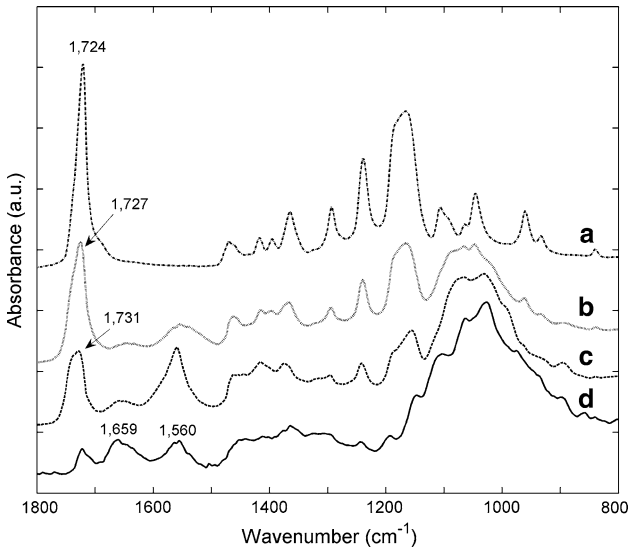

Fig. 5 ATR–FTIR spectra of **a** pure PCL **b** chitosan/PCL (50/50 wt%) **c** chitosan/PCL (75/25 wt%) and **d** pure chitosan

PCL, whereas the absorption peak of PCL was better expressed in the 50 wt% PCL blends.

The potential molecular interaction of two components is the formation of amide bond (C–N) between the ester group of PCL and the amine group of chitosan. In such a case, the absorption peak of carbonyl stretch would shift from 1,724 to 1,630–1,680 cm^{-1}, meanwhile the two peaks corresponding to amine group of chitosan would convert to one weak band as the primary amine changes to secondary form [31]. However, in our study, these changes were not observed in the FTIR spectra. The peak absorption of the C–N bond stretch in the possible formed amide bond could not be differentiated from the existing C–N bonds in chitosan at 1,000–1,350 cm^{-1} [31]. All the results indicated that there was no chemical bonding between chitosan and PCL in the fabricated composite and they only physically coexisted. Interestingly, the peak absorption of carbonyl stretch of PCL in the composite containing 25 and 50 wt% PCL was at 1,731 and 1,727 cm^{-1}, respectively, while for pure PCL was at 1,724 cm^{-1}. The peak shift might be caused by the existence of the surfactant span-80 since it has strong carbonyl band absorbance at 1,740 cm^{-1}. However, the absorbance peak of carbonyl band from span-80 was possibly overlapped with the one of PCL and difficult to be detected with ATR–FTIR single scan. According to the shift number, it can be deduced that the presence of the surfactant in the measurement area of the composite with 25 wt% PCL was higher than that with 50 wt% PCL.

3.4 FTIR spectroscopic imaging

The homogeneity and uniformity of composite hydrogels were determined using ATR–FTIR images with an FPA detector. The integrated absorbance of characteristic band for each compound was plotted to demonstrate its distribution in a composite. It is critical to identify characteristic spectral bands for each component that can be used for constructing images for the distribution of a specific polymer. The amide II band at 1,560 cm^{-1} (range used for generating the image was 1,617–1,490 cm^{-1}) and the carbonyl band at 1,727 cm^{-1} (1,740–1,710 cm^{-1}) were used to characterise chitosan and PCL, respectively. The surfactant span-80 (5 v/v%) which was used as the emulsifier in this study was also detected within wavenumbers ranging from 1,750 to 1,735 cm^{-1}. As shown in Fig. 6, the distribution of chitosan and PCL in both 25 and 50 wt% PCL composites was uniform at both surface and cross sections. Comparing the images generated for the specimen containing 25 wt% PCL to the one with 50 wt% PCL, the reduction in amide II group absorbance was observed, which was attributed to the decrease of the content of chitosan in the blends. Meanwhile the absorbance of the corresponding band of PCL was apparently enhanced from 25 wt% specimen to 50 wt% one as a result of the increasing PCL concentration. The absorbance of the corresponding band of surfactant in the composite with 25 wt% PCL was significantly higher than the one with 50 wt% PCL, which was consistent with the carbonyl peak shift shown in Fig. 5. This effect may be attributed to the emulsion process; creation of micropores with smaller size on the walls of the pores at 25 wt% PCL concentration depicted in Fig. 3 enhances the surface area, subsequently increases the amount of surfactant on the pore surfaces per volume of the sample used for characterisation by ATR–FTIR imaging as observed in Fig. 6. The surfactant span-80 used in this system is non-toxic and has been widely used in food industry. Moreover, it has been applied into the preparation of superporous hydrogel composite and microemulsions for drug delivery [32–34]. The residue of small amount of this surfactant in the composites had negligible effect on cell viability.

3.5 Swelling of composite hydrogels

In vitro nutrients supply and waste exchange relies on the swelling property of hydrogels. Pure chitosan hydrogel exhibited a swelling ratio of 17.2 ± 1.4 in PBS at 37°C that is comparable with the values reported in the previous studies [35–37]. The swelling ratio of the chitosan/PCL hydrogels was decreased due to the introduction of hydrophobic PCL segment. As shown in Fig. 7 the swelling ratio was decreased by 11 and 32% for 25 and 50 wt% PCL, respectively.

3.6 Mechanical properties

Adequate mechanical strength is critical for hydrogels in tissue engineering applications. Compressive test was used

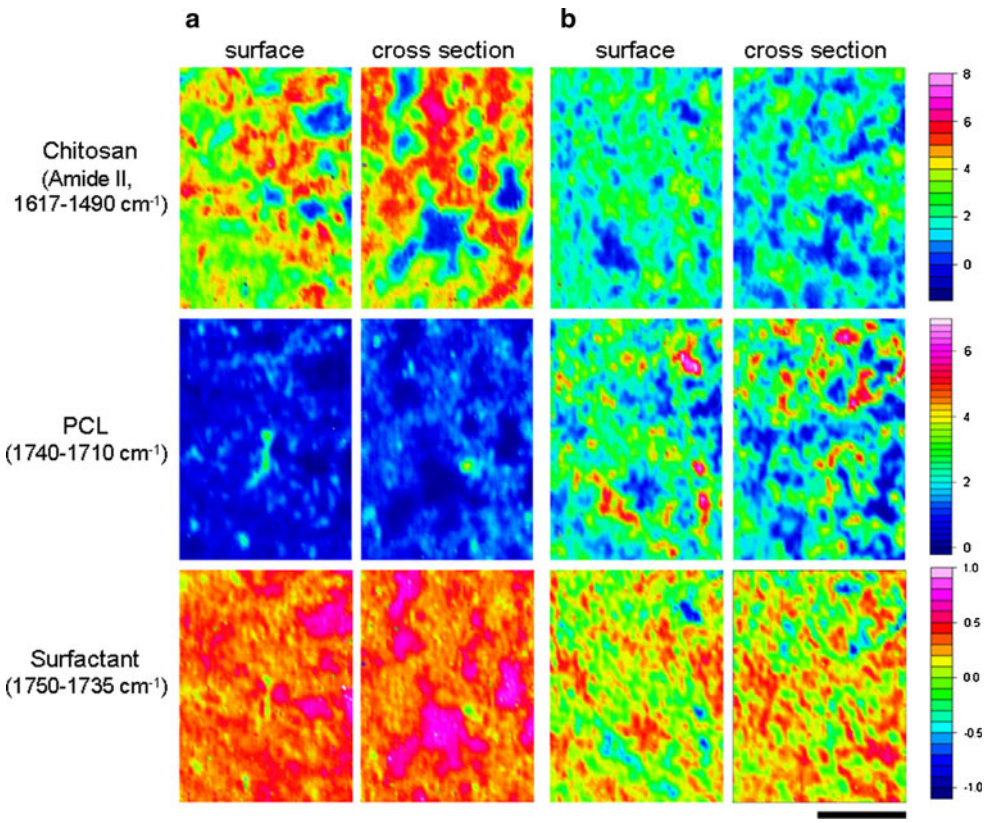

Fig. 6 FTIR imaging of chitosan/PCL composite hydrogels with **a** 25 wt% PCL and **b** 50 wt% PCL. *Scale bar* showing a length of 350 μm

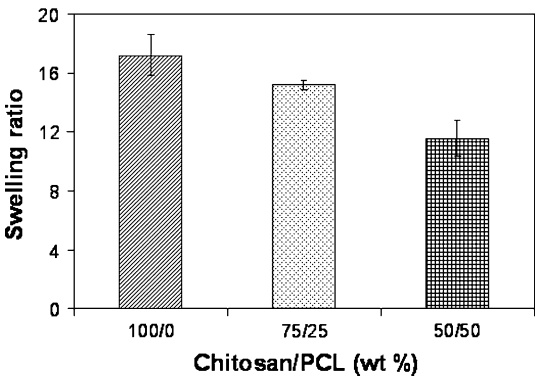

Fig. 7 Swelling ratio of the composite hydrogels with various compositions

for wet composite hydrogels, and tensile test was performed for the dried specimens. Increasing the concentration of PCL enhanced the compressive properties of chitosan composites. As shown in Table 2, compared with pure chitosan, the compressive modulus of composite hydrogels were increased 160 and 290%, for 25 and 50 wt% PCL, respectively. Similar trend was observed for PVA/PCL composites in the previous reported study; increasing PCL concentration, promoted the mechanical performance of composite hydrogels. However, when the PCL content was increased to 75 wt%, the compressive modulus of PCL/PVA was reduced dramatically because of

Table 2 Mechanical properties of chitosan/PCL composites compared to the pure chitosan hydrogel

Chitosan/PCL (wt%)	Compressive modulus (KPa)	Tensile modulus (MPa)
100/0	8.6 ± 1.2	0.55 ± 0.06
75/25	21.9 ± 1.7	1.23 ± 0.14
50/50	32.9 ± 2.2	1.44 ± 0.08

phase inversion and formation of PCL as a continuous phase [16]. The result of this study was in agreement with the PCL/PVA system. As shown in Fig. 2, with 75 wt% PCL, the specimen was soft and fragile. The addition of PCL remarkably enhanced the tensile properties and mechanical strength of chitosan hydrogels (Table 2). The tensile modulus of porous chitosan hydrogel was 0.55 MPa for samples with random pore distribution and average pore size of 137 μm. The results of previous studies demonstrated that the mechanical property of porous chitosan hydrogels relies on pore size and orientation [6]. The elastic modulus of porous chitosan membrane was reduced to 0.1–0.5 MPa compared to non-porous chitosan membranes, which were 5–7 MPa and the highest extensibility (maximum strain) was achieved with a random pore orientation structure and 120 μm pore size [6]. The composite hydrogels produced in this study can potentially be

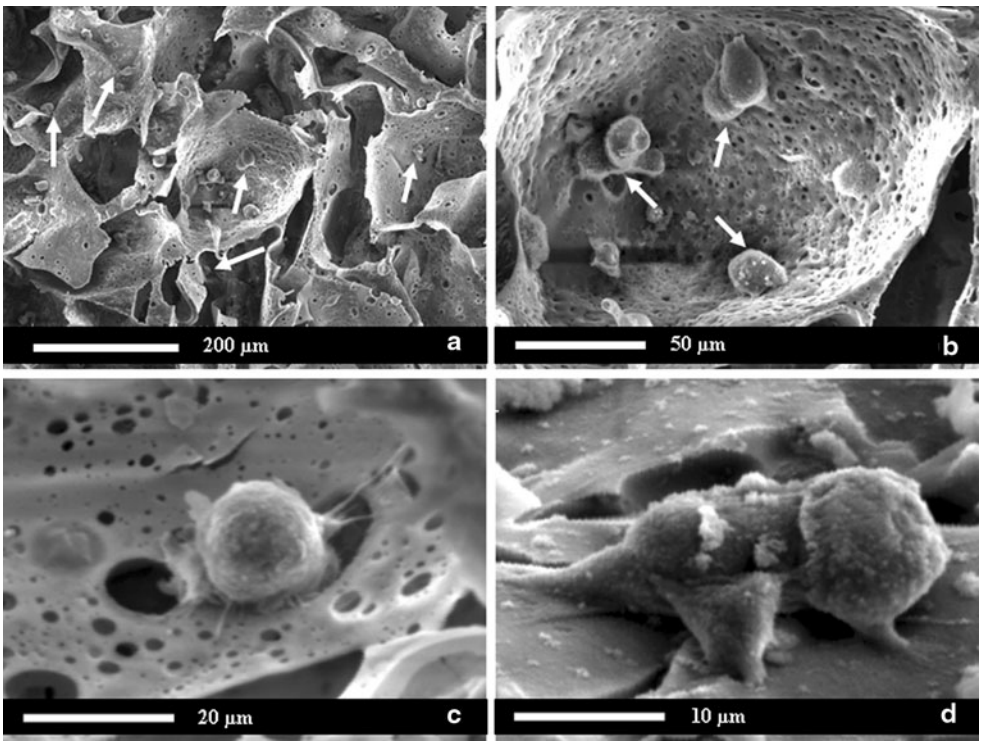

Fig. 8 SEM image of fibroblast cells grown on **a–c** chitosan/PCL (75/25 wt%) composite and **d** pure chitosan hydrogel for one day

used for engineering tissues such as skin and cartilage repair because of improved mechanical properties.

3.7 In vitro cell culture test

In vitro cell culture test was performed to assess the biocompatibility of the chitosan/PCL composites processed by method developed in this study. The SEM images (Fig. 8a–d) of samples after 24 h cell seeding show that the fibroblast cells started to adhere on the surface of hydrogels. The cells on the composite hydrogels presented similar morphology compared to the one attached on the surface of pure chitosan hydrogel. Interestingly the micropores of composite hydrogels seemed to favour the cell attachment as shown in Fig. 8b, c. CLSM images in Fig. 9a, c and e show that after cell culturing for 3 days, cells uniformly distributed on the hydrogels surface and almost all the cells were alive. However, the cells proliferation in the hydrogels containing 50 wt% PCL was slower than others. After 7 days, fibroblast cells stretched and formed confluent monolayers on the surfaces of the composite and pure chitosan hydrogels (Fig. 9b, d, f). The cell proliferation on the 25 wt% PCL was more efficient than the others. Cell attachment is the function of both chemical and physical properties of the 3D hydrogel. Cell migration and subsequent proliferation is determined by substrate mechanical strength, pore size and surface topography [38]. Berry et al. reported that fibroblast cell attachment was improved by the existence of small sized pits (7 μm) on the scaffold surface which provided footholds for cells to gain mechanical adhesion [39]. Therefore, the abundant micron sized pores (4.4–7.1 μm) on the composite hydrogels might boost the cells attachment as observed in Fig. 8c, hence improving the cells proliferation. However, the cells proliferation in 50 wt% PCL composite was lower and the amount of dead cells was noticeably higher compared to pure chitosan and composite with 25 wt% PCL. This effect might be resulted from the hydrophobic properties of PCL, which decreased the media capture capability and cell recognition signals. The promising cell viability results demonstrated that the composites fabricated by sonication emulsion followed by lyophilisation were biocompatible. A small quantity of cells penetrated into the pores and grew along the pore walls, indicating either pore architecture or material surface properties needs further optimisation to promote cell infiltration.

4 Conclusions

The emulsion followed by lyophilisation process was an efficient technique to fabricate chitosan/PCL composite hydrogels. Sonication was an efficient technique for the preparation of stable emulsion. The mechanical properties

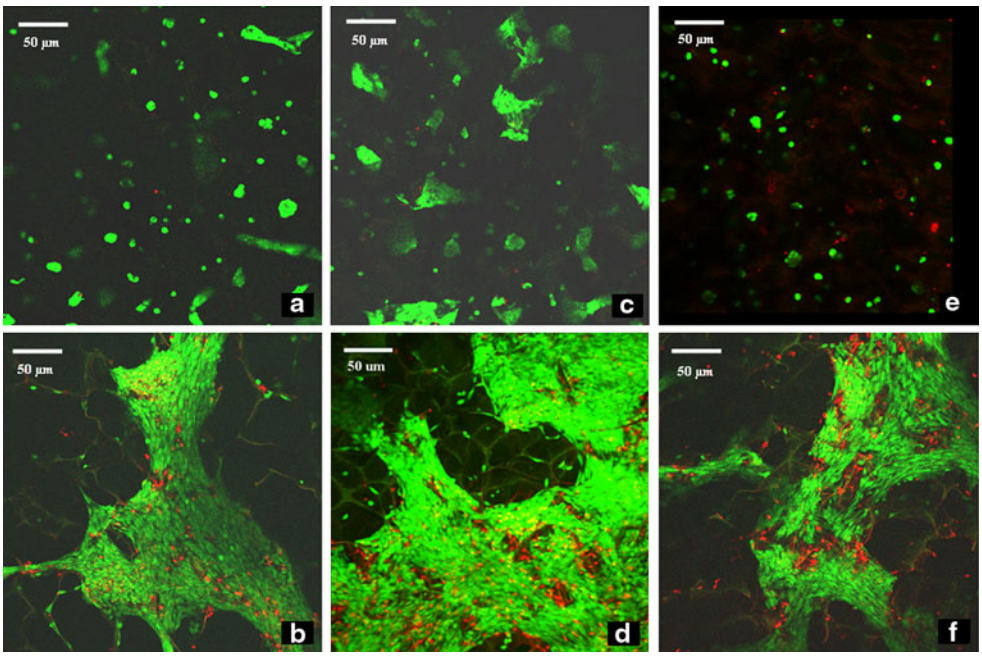

Fig. 9 CLSM image of fibroblast cells grown on **a**, **b** chitosan **c**, **d** chitosan/PCL (75/25 wt%) composite **e**, **f** chitosan/PCL (50/50 wt%) composite for 3 and 7 days, respectively

was enhanced by increasing the concentration of PCL to 50%, however, further increase of PCL concentration resulted in production of soft and fragile composite that was not suitable for hydrogel fabrication. The method used in this study allows fabricating homogenous mixtures of composites with micro-sized pores on the walls of larger pores. The high cell viability and proliferation confirmed the superior biocompatibility of the composite hydrogels. In conclusion, the chitosan/PCL composite hydrogels with maximum 50 wt% PCL exhibited great potential for tissue engineering applications. Future study will be conducted to increase the size of the pores and improve cell proliferation.

Acknowledgment The authors acknowledge the support of Miss Tsun Ting Lo for carrying a part of experimental study and financial support from ARC Grant no. DP0988545.

References

1. Khademhosseini A, Langer R. Microengineered hydrogels for tissue engineering. Biomaterials. 2007;28(34):5087–92.
2. Ma PX. Biomimetic materials for tissue engineering. Adv Drug Deliv Rev. 2008;60(2):184–98.
3. Sarasam A, Madihally SV. Characterization of chitosan-polycaprolactone blends for tissue engineering applications. Biomaterials. 2005;26(27):5500–8.
4. Wan Y, Wu H, Cao X, Dalai S. Compressive mechanical properties and biodegradability of porous poly(caprolactone)/chitosan scaffolds. Polym Degrad Stab. 2008;93(10):1736–41.
5. Gallico GG, 3rd, O'Connor NE, Compton CC, Remensnyder JP, Kehinde O, Green H. Cultured epithelial autografts for giant congenital nevi. United States: Shriners Burns Institute, Boston; 1989.
6. Suh JK, Matthew HW. Application of chitosan-based polysaccharide biomaterials in cartilage tissue engineering: a review. Biomaterials. 2000;21(24):2589–98.
7. Madihally SV, Matthew HWT. Porous chitosan scaffolds for tissue engineering. Biomaterials. 1999;20(12):1133–42.
8. Averousa L, Moro L, Dole P, Fringant C. Properties of thermoplastic blends: starch-polycaprolactone. Polymer. 2000;41:4157–67.
9. Zhu H, Ji J, Lin R, Gao C, Feng L, Shen J. Surface engineering of poly(D, L-lactic acid) by entrapment of chitosan-based derivatives for the promotion of chondrogenesis. J Biomed Mater Res. 2002;62(4):532–9.
10. Kweon HY, Yoo MK, Park IK, Kim TH, Lee HC, Lee HS, et al. A novel degradable polycaprolactone networks for tissue engineering. Biomaterials. 2003;24:801–8.
11. Garcia Cruz DM, Coutinho DF, Mano JF, Gomez Ribelles JL, Salmeron Sanchez M. Physical interactions in macroporous scaffolds based on poly(ε-caprolactone)/chitosan semi-interpenetrating polymer networks. Polymer. 2009;50(9):2058–64.
12. Wan Y, Xiao B, Dalai S, Cao X, Wu Q. Development of polycaprolactone/chitosan blend porous scaffolds. J Mater Sci Mater Med. 2009;20:719–24.
13. Honma T, Senda T, Inoue Y. Thermal properties and crystallization behaviour of blends of poly(ε-caprolactone) with chitin and chitosan. Polym Int. 2003;52:1839–46.
14. Sarasam AR, Samli AI, Hess L, Ihnat MA, Madihally SV. Blending chitosan with polycaprolactone: porous scaffolds and toxicity. Macromol Biosci. 2007;7(9–10):1160–7.
15. She H, Xiao X, Liu R. Preparation and characterization of polycaprolactone-chitosan composites for tissue engineering applications. J Mater Sci. 2007;42(19):8113–9.
16. Mohan N, Nair PD. Polyvinyl alcohol-poly(caprolactone) semi IPN scaffold with implication for cartilage tissue engineering. J Biomed Mater Res Part B Appl Biomater. 2007;84:584–94.

17. Van der Weerd J, Chan K, Kazarian SG. An innovative design of compaction cell for in situ FTIR imaging of tablet dissolution. Vib Spectrosc. 2004;35:9–13.
18. Kazarian SG, Chan KLA. Micro- and macro-attenuated total reflection Fourier transform infrared spectroscopic imaging. Appl Spectrosc. 2010;64:135A–52A.
19. Palombo F, Weinberg PD, Kazarian SG. Measurement of drug and macromolecule diffusion across atherosclerotic rabbit aorta ex vivo by attenuated total reflection-fourier transform infrared imaging. J Biomed Opt 2009; 14: 044008.
20. Dehghani F, Annabi N, Valtchev P, Mithieux SM, Weiss AS, Kazarian SG, et al. Effect of dense gas CO_2 on the coacervation of elastin. Biomacromolecules. 2008;9:1100–5.
21. Chan K, Govada L, Bill R, Chayen N, Kazarian SG. Attenuated total reflection-FTIR spectroscopic imaging of protein crystallization. Anal Chem. 2009;81:3769–75.
22. Xu Q, Nakajima M, Ichikawa S, Nakamura N, Shiin T. A comparative study of microbubble generation by mechanical agitation and sonication. Innov Food Sci Emerg. 2008;9:489–94.
23. Arirachakaran S, Oglesby KD, Malinowsky MS, Shoham O, Brill JP. An analysis of oil/water flow phenomena in horizontal pipes. SPE Production Operations Symposium Oklahoma City, 1989.
24. Yeo LY, Matar OK, Perez Susana, de Ortiz E, Hewitt GF. A description of phase inversion behaviour in agitated liquid–liquid dispersions under the influence of the Marangoni effect. Chem Eng Sci. 2002;57:3505–20.
25. Seol YJ, Lee JY, Park YJ, Lee YM, Ku Y, Rhyu IC, et al. Chitosan sponges as tissue engineering scaffolds for bone formation. Biotechnol Lett. 2004;26(13):1037–41.
26. Doillon C, Whyne C, Brandwein S, Silver F. Collagen-based wound dressings: control of the pore structure and morphology. J Biomed Mater Res. 1986;20:1219–28.
27. O'Brien FJ, Harley BA, Yannas IV, Gibson LJ. The effect of pore size on cell adhesion in collagen-GAG scaffolds. Biomaterials. 2005;26(4):433–41.
28. Jain S, Bates F. On the origins of morphological complexity in block copolymer surfactants. Science. 2003;300:460–4.
29. Osman Z, Arof AK. FTIR studies of chitosan acetate based polymer electrolytes. Electrochim Acta. 2003;48(8):993–9.
30. Senda T, He Y, Inoue Y. Biodegradable blends of poly(ε-caprolactone) with α-chitin and chitosan: specific interactions thermal properties and crystallization behaviour. Polym int. 2001;51:33–9.
31. Sarasam AR, Krishnaswamy R, Madihally S. Blending chitosan with polycaprolactone: effects on physicochemical and antibacterial properties. Biomacromolecules. 2006;7:1131–8.
32. Forsberg F, Liu J, Patel M, Liu L, Lin L, Solis C, et al. Preclinical acute toxicology study of surfactant-stabilized ultrasound contrast agents in adult rats. Int J Toxicol. 2010;29:32–9.
33. Chavda H, Patel C. Preparation and characterization od swellable polymer-based superporous hydrogel composite of poly(acrylamide-co-acrylic acid). Trends Biomater Artif Organs. 2010;24:83–9.
34. Karasulu H. Microemulsions as novel drug carriers: the formation, stability, applications and toxicity. Expert Opin Drug Deliv. 2008;5:119–35.
35. Kathuria N, Tripathi A, Kar KK, Kumar A. Synthesis and characterization of elastic and macroporous chitosan-gelatin cryogels for tissue engineering. Acta Biomater. 2009;5:406–18.
36. Tan H, Chu Constance R, Payne KA, Marra Kacey G. Injectable in situ forming biodegradable chitosan-hyaluronic acid based hydrogels for cartilage tissue engineering. Biomaterials. 2009;30:2499–506.
37. Huang Y, Onyeri S, Siewe M, Moshfeghian A, Madihally SV. In vitro characterization of chitosan-gelatin scaffolds for tissue engineering. Biomaterials. 2005;26(36):7616–27.
38. Hatson W, Shields J, Wilkinson P. Lymphocyte locomotion and attachment on two-dimensional surfaces and in three-dimensional matrices. J Cell Biol. 1982;92:747–52.
39. Berry CC, Campbell G, Spadiccino A, Robertson M, Curtis ASG. The influence of microscale topography on fibroblast attachment and motility. Biomaterials. 2004;25:5781.